

# Cyclic Oxidation and Hot Corrosion Behavior of Y/Cr-Modified Aluminide Coatings Prepared by a Hybrid Slurry/Pack Cementation Process

Jintao Lu · Shenglong Zhu · Fuhui Wang

Received: 6 July 2010/Revised: 20 September 2010/Published online: 18 December 2010  
© Springer Science+Business Media, LLC 2010

**Abstract** Y/Cr-modified aluminide coatings were prepared on a Ni-base superalloy K417G using a hybrid slurry/pack cementation process. The coatings consisted of a NiAl layer with dissolved Cr and Y. The microstructures and high temperature corrosion behavior of the coatings were characterized using SEM/EDS, XRD, EPMA and SIMS. Cyclic oxidation tests at 1000 °C for 200 h were carried out in air. The results indicated that specimens coated by either the Y/Cr-modified aluminide coatings or the simple aluminide coatings exhibited better oxidation resistances than the cast alloy. The Y/Cr-modified aluminide coatings possessed lower oxidation rates and better degradation resistance than the simple aluminide coatings during the oxidation tests. Furthermore, the alumina scales formed on the Y/Cr-modified aluminide coatings were considerably more adherent than those on the simple aluminide coatings during the thermal cycling. The hot corrosion tests consisted of applying a 25 wt%  $K_2SO_4$  +75 wt%  $Na_2SO_4$  salt mixture to the specimens and exposing at 900 °C. The Y/Cr-modified aluminide coatings showed the longest service life compared with the cast alloy and aluminide coatings, which suffered significant sulfur attack. After 200 h, the Y/Cr-modified aluminide coatings were still protective.

**Keywords** Y/Cr-modified aluminide coating · Pack cementation process · Slurry · Oxidation · Hot corrosion

---

J. Lu (✉) · S. Zhu · F. Wang  
State Key Laboratory for Corrosion and Protection, Institute of Metal Research, Chinese Academy of Science, Wencui Road 62#, Shenyang City 110016, People's Republic of China  
e-mail: jtlu@imr.ac.cn

## Introduction

Coatings have been used to serve as physical barriers between aggressive environments and the substrates since they were first applied to high pressure turbine airfoils in the early 1960s. There are essentially two types of high temperature coatings: diffusion coatings, such as aluminized coating, and overlay coatings, such as MCrAlY coating [1]. Currently, the generation of MCrAlY coatings as well as those emerging from TBC technologies has been extensively applied to the hot components of gas turbine [2]. Electron-beam physical deposition (EB-PVD), low pressure plasma spray (LPPS), magnetron sputtering and arc ion plating (AIP) are the most frequently used methods to deposit MCrAlY coatings [3–6]. Their main drawback, however, is the so-called line-of-sight effect, which results in coarse microstructures and a non-uniform coating thickness when depositing to complex-shaped components. Also, the high cost of these methods restricts the MCrAlY coating from wider applications.

In fact, the diffusion coatings such as simple, Cr- or Pt-modified aluminide coatings prepared by pack cementation or chemical vapor deposition (CVD) have been widely used for many years and they are still proving to be extremely useful in certain areas. It is estimated that more than 80% of all airfoils are coated by those methods [1]. Costa et al. [7, 8] carried out a series of studies on the co-deposition of Cr–Al coatings. Xiang et al. [9] discussed the pack thermodynamics of the co-deposition of Cr–Al and Si–Al coatings to give the theoretical foundation of these coating techniques. The simple or Cr-modified aluminide coatings are prone to oxide scale spallation, while the Pt-modified aluminide coatings are expensive. Thus, reactive element (RE)-modified aluminide coatings have attracted the interest of investigators. Usually, RE are introduced into coatings by ion implantation. NiAl coatings modified by Y and Ce were prepared using this method by Jedlinski et al. [10], and possessed good oxide scale adherence. However, it is difficult to prepare Y-containing coatings by diffusion methods for the following reasons. First, Y atoms with a large atomic radius, nearly double that of Ni, are very slow to diffuse into the Ni based alloys. Second, considering the high activity with oxygen for Y and the more negative formation free energy of  $Y_2O_3$  than  $Al_2O_3$ , yttrium powders react preferentially with alumina to form yttria during the pack cementation process. Replacement of alumina powders with yttria powders when preparing a Y-containing coating by pack cementation was feasible [11], but is obviously not economical.

The pack cementation, and slurry processes are the most frequently used methods to prepare diffusion coatings due to their low cost and elimination of the line-of-sight effect [12]. Therefore, producing a Y–Cr–Al-containing coating by diffusion methods, which is free of the line-of-sight effect, is quite significant. Previously, the Y-modified aluminide coatings have been prepared on IN738 superalloy using a slurry technique [13]. They had better hot corrosion resistance than the simple aluminide coatings. In the present study, Y/Cr-modified aluminide coatings were prepared using a hybrid slurry/pack cementation technique and their cyclic oxidation and hot corrosion behavior were investigated. For comparison, aluminide coatings were prepared on the same cast alloy.

## Experimental Procedures

### Material

The nickel-based superalloy K417G, which was prepared by vacuum-induction casting, was used as the substrate. Its nominal composition was shown in Table 1. Rectangular specimens with the dimension of  $10 \times 15 \times 2$  mm were cut from the cast ingot. These specimens were ground to an 800-grit finish and then ultrasonically cleaned in acetone before the co-deposition processes.

### Coating Preparation

Y/Cr-modified aluminide coatings were prepared by a hybrid slurry/pack cementation process. Firstly, a special Y-containing slurry was sprayed on the specimens to a thickness of  $\sim 1$  mm, then dried at  $100$  °C for 1 h. Secondly, the slurry-coated specimens were embedded in a Cr-containing powder mixture, followed by the heat treatment at  $1050$  °C for 40 min. Thirdly, aluminization was carried out at  $1000$  °C for 4 h. Both the chromization and aluminization were performed in an argon atmosphere. The slurry consisted of Y,  $Y_2O_3$ , catalyst and organic solvent. The composition of the powder mixture for chromization was: 30 wt% Cr, 8 wt% Ni, 2 wt%  $NH_4Cl$  and 60 wt%  $Al_2O_3$ , and that for aluminization was: 99 wt% FeAl and 1 wt%  $NH_4Cl$ . Simple aluminide coatings were deposited by pack cementation at  $950$  °C for 4 h using the same aluminization pack powders.

### Oxidation Tests

The cyclic oxidation tests were carried out in a tube furnace at  $1000$  °C. In each cycle, the specimens were put in the furnace for 60 min, followed by cooling down to room temperature for 10 min. Three samples of each type were used under the same test conditions and the oxidation kinetics curves were plotted using the average mass change. The mass changes of the specimens were measured using an electrobalance with a detection limit of 0.01 mg.

### Hot Corrosion Tests

The hot corrosion tests in the present study were performed at  $900$  °C. Before exposure, specimens were preheated, followed by depositing a water-saturated solution of 25 wt%  $K_2SO_4$  +75 wt%  $Na_2SO_4$  on the surface. The amount of salt

**Table 1** Nominal composition of the cast alloy K417G (wt%)

C	Cr	Co	Al	Mo	Ti	Fe	V	B	Zr	Ni
0.13	8.5	9	4.8	2.5	4.1	0.4	0.6	0.013	0.05	Bal
–	–	–	–	–	–	–	–	–	–	–
0.22	9.5	11	5.7	3.5	4.7	1	0.9	0.024	0.09	–

deposited was  $\sim 2 \text{ mg/cm}^2$ . The specimens were taken out, cleaned, weighed and recoated with salt every 20 h. The hot corrosion kinetics was determined by the average mass change of three identical samples.

### Analytical Characterization

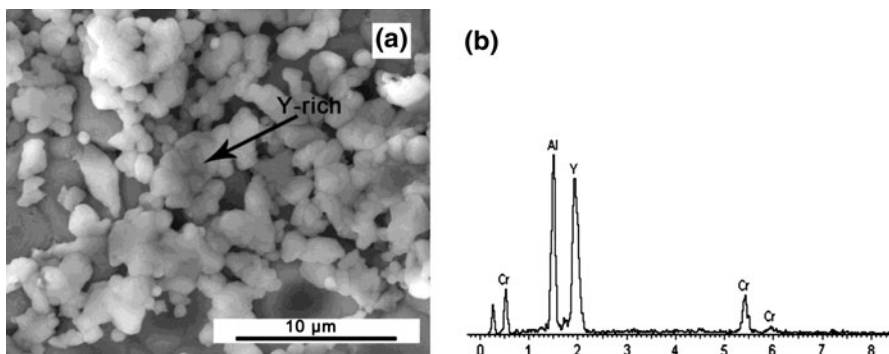
The surface and cross-sectional morphologies of the specimens were observed by the scanning electron microscopy (SEM). Semi-quantitative chemical compositions of the specimens were obtained by the energy dispersive spectrometry (EDS). X-ray diffraction was used to identify the phases of the coatings and the oxide scales. Electron micro-probe analysis (EPMA) was used to characterize the elemental concentrations after hot corrosion. Secondary ion mass spectrometry (SIMS) was used to profile the yttrium in the Y/Cr-modified aluminide coating.

## Results

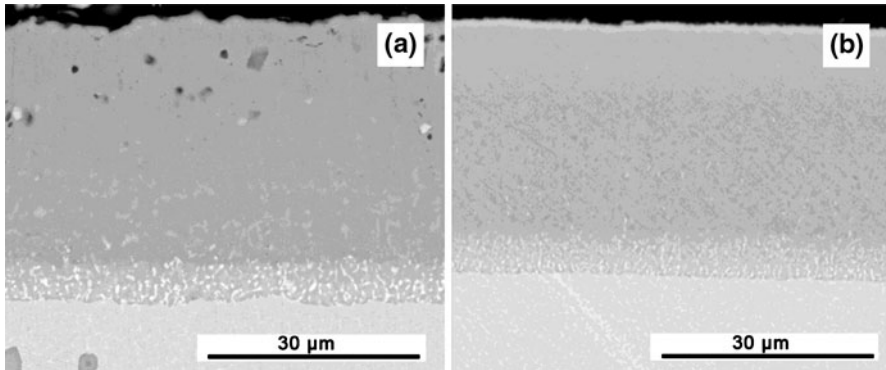
### Composition and Microstructures of Coatings

Figure 1a shows the surface morphology of the specimen after chromization. A co-deposited Y–Cr coating formed on the substrate. White particles formed on the surface of the chromized layer, as indicated by an arrow in Fig. 1a. According to EDS analysis (Fig. 1b), high contents of Al and Y were detected. But, XRD result indicated that the main phase of the coating was  $\text{Ni}_2\text{Cr}_3$ . No Y-containing phase was detected, which showed that the amount of the Y-containing phase was trace.

A cross-sectional image of the Y/Cr-modified aluminide coating is presented in Fig. 2a. After aluminization, the above-mentioned Y–Cr layer was totally dissolved. Two zones formed in the Y/Cr-modified aluminide coating. The outer zone was  $\sim 50 \mu\text{m}$  and an interdiffusion zone was  $\sim 8 \mu\text{m}$ . The average chemical composition of the outer zone was measured to be 36.1Al–0.7Ti–16.7Cr–5.5Co–41.4Ni (wt%). Some alumina powders were trapped in the outer zone. NiAl was the main



**Fig. 1** Surface morphology (a) and energy dispersive analysis by X-rays (b) of the co-deposited Y–Cr coating

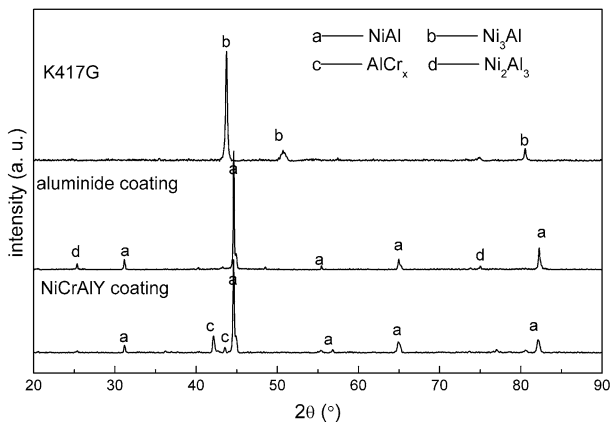


**Fig. 2** Cross-sectional morphologies of the coatings, **a** Y/Cr-modified aluminide coating, **b** aluminide coating

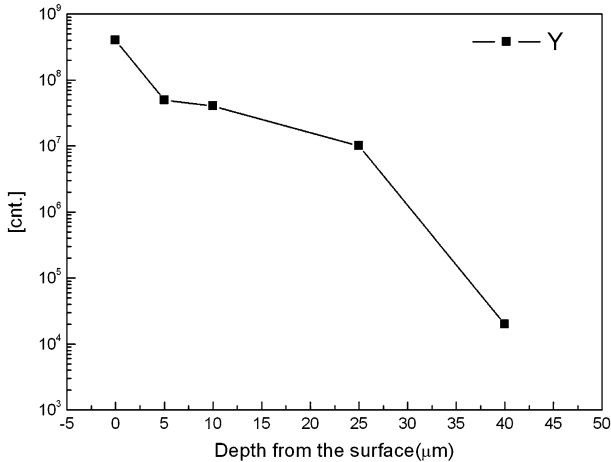
phase according to the XRD result shown in Fig. 3. At the same time, a few of weak peaks of  $\text{AlCr}_x$  phase were observed.

Figure 2b shows the cross-sectional image of the aluminide coating. This coating consisted of an outward-grown NiAl phase (shown in Fig. 3) with a thickness of  $\sim 50 \mu\text{m}$  and an interdiffusion zone with a fine dispersion of second-phase particles resulting from the outward diffusion of Ni. Substrate components such as Cr, Co and Ti diffused into the coating, which is inevitable for a diffusion coating. The average composition of the outer layer was measured to be  $34\text{Al}-1.4\text{Ti}-3.8\text{Cr}-7.2\text{Co}-53.6\text{Ni}$  (wt%).

Figure 4 illustrates the distribution of yttrium in the Y/Cr-modified aluminide coating, as determined by SIMS analysis. It confirmed the existence of yttrium in the coating, also its exponentially decreasing distribution from the surface of the coating to the interior.



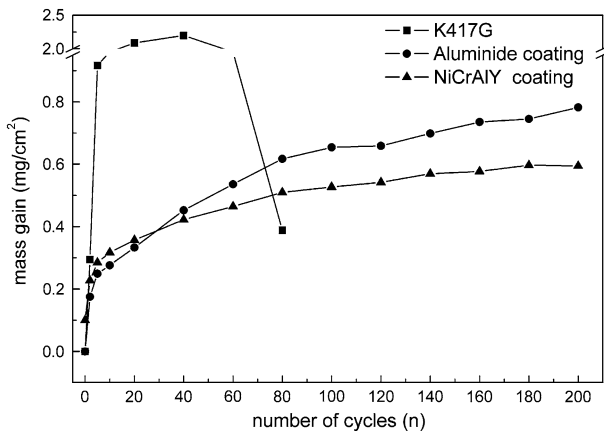
**Fig. 3** XRD patterns of the cast alloy and the coatings



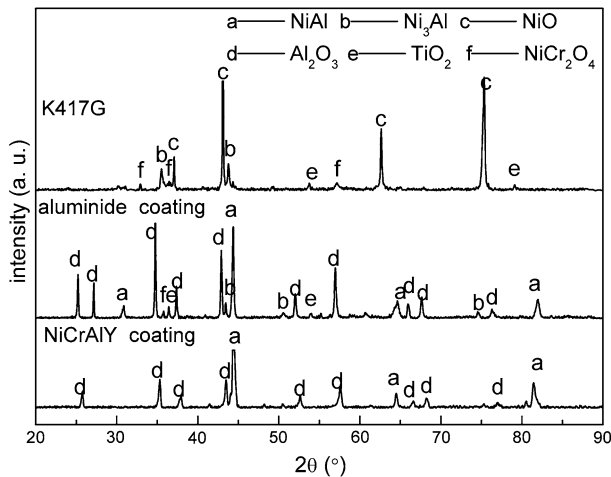
**Fig. 4** The distribution of the yttrium by SIMS

### Oxidation Behavior

Figure 5 presents the cyclic oxidation kinetics of the cast alloy and the two coated specimens at 1000 °C. The mass gain of the cast alloy rose to a maximum after 40 cycles, followed by a serious mass loss due to spallation. Some fluctuations were observed in the mass-gain curve for the aluminide coating, indicating that spallation occurred and new oxide scale grew on the exposed surface. The Y/Cr-modified aluminide coating showed better cyclic oxidation resistance. The mass-gain curve followed the parabolic rate law, with a parabolic rate constant of  $\sim 1.68 \times 10^{-3} \text{ mg}^2 \text{ cm}^{-4} \text{ h}^{-1}$ . In the initial stage, however, the oxidation rate of the Y/Cr-modified aluminide coating was a little higher than that of the aluminide coating.



**Fig. 5** Cyclic oxidation kinetics of the alloy and the coatings at 1000 °C



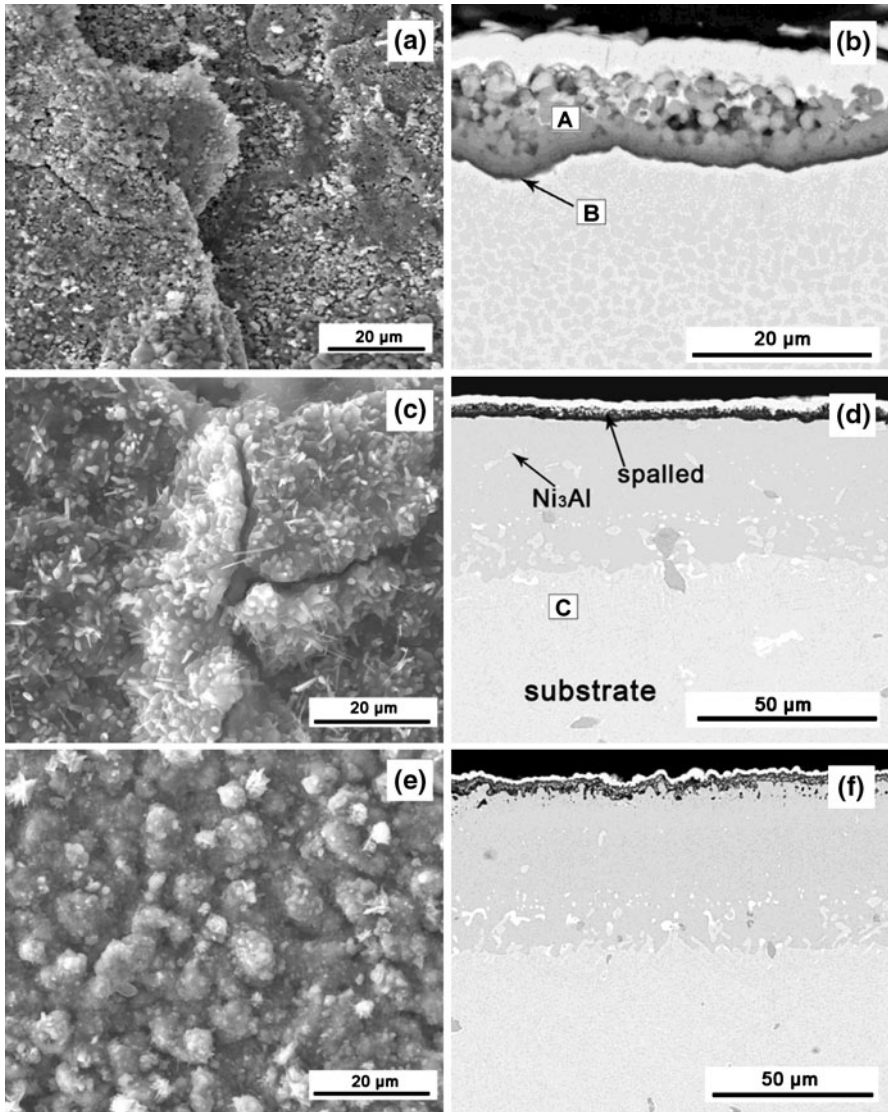
**Fig. 6** XRD patterns of the cast alloy and the coatings after cyclic oxidation

Figure 6 shows the XRD patterns of the specimens after cyclic oxidation. A large amount of NiO and a small amount of TiO<sub>2</sub> and NiCr<sub>2</sub>O<sub>4</sub> spinel formed on the surface of the cast alloy. For both the coatings, Al<sub>2</sub>O<sub>3</sub> was the main phase in the oxide scales, and β-NiAl was the dominant phase in the coatings. However, some TiO<sub>2</sub> and Ni<sub>3</sub>Al were detected for the aluminide coatings.

The surface and cross-sectional morphologies of the cast alloy and the two coated specimens after cyclic oxidation are shown in Fig. 7. For the cast alloy, the oxide scale showed cracks and spallation after 80 cycles (Fig. 7a). EDS combined with the XRD results indicated that the exposed area (Area A) underlying the Ni plating in Fig. 7b was NiO which contained some NiCr<sub>2</sub>O<sub>4</sub> and Ti-rich oxide particles, and an inner region (Area B) of Cr-rich oxides.

Some cracks and spallation of the oxide scales on the aluminide coating were observed (Fig. 7c). However, both the spalled and unspalled areas, according to EDS, were mainly Al-rich oxides. It confirmed again that new Al<sub>2</sub>O<sub>3</sub> scale formed on the exposed surface. The same spalled features were also observed from the cross-sectional image, indicated by the non-uniform oxide scale thickness (Fig. 7d). The scale thickness was about 8 μm. Island-like Ni<sub>3</sub>Al was observed in the coating, surrounded by β-NiAl phases. An obvious interdiffusion zone (Area C) appeared between the coating and substrate. Second-phases, revealed as bright particles rich in Cr, Ti, and Mo, were precipitated in the interdiffusion layer.

No significant degradation of the Y/Cr-modified aluminide coating was observed during testing for 200 cycles. The oxide scales were fine grained and thin, with the average thickness about 5 μm, and no spallation was observed (Fig. 7e, f). Thus the Y/Cr-modified aluminide coating possessed the best cyclic oxidation resistance at 1000 °C.



**Fig. 7** Surface and cross-sectional morphologies of the alloy and the coatings after cyclic oxidation, **a**, **b** cast alloy for 100 cycles, **c**, **d** aluminide coating for 200 cycles, **e**, **f** Y/Cr-modified aluminide coating for 200 cycles

### Hot Corrosion Behavior

Figure 8 illustrates the kinetics of the specimens deposited with the salt mixture at 900 °C. The cast alloy suffered dramatic damage, as indicated by a linear increase of mass gain in the first 20 h, followed by a rapid mass decrease. The aluminide coating also exhibited a high corrosion rate. After 40 h, a linear drop appeared due



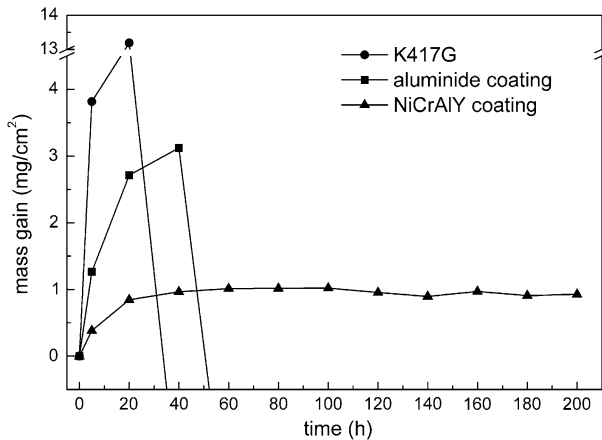


**Fig. 8** Hot corrosion kinetics of the alloy and the coatings

to the spallation of oxide scales, followed by the destruction of the coating. The mass gain of the Y/Cr-modified aluminide coating was approximately steady during the whole test. Such a result indicates that the oxide scale formed on the coating surface effectively protected the metal from further corrosion.

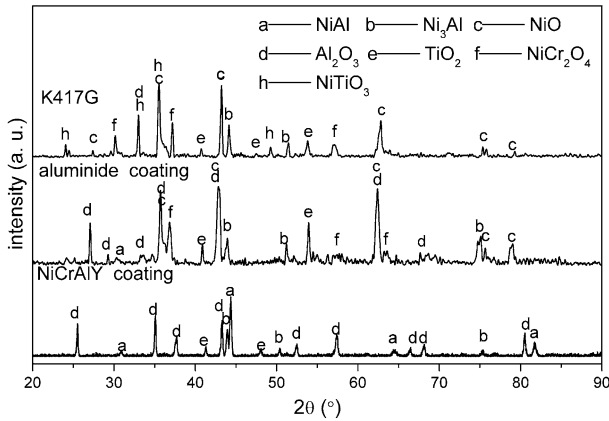
XRD patterns of the specimens after hot corrosion are presented in Fig. 9. For the cast alloy, mixed oxide scales formed after 20 h. Peaks of NiO, Al<sub>2</sub>O<sub>3</sub>, NiCr<sub>2</sub>O<sub>4</sub> spinel and Ti-rich oxides were detected. The oxides formed on the aluminide coating were identified as Al<sub>2</sub>O<sub>3</sub> together with TiO<sub>2</sub>, NiO and NiCr<sub>2</sub>O<sub>4</sub> spinel. The intensity of  $\beta$ -NiAl peaks was weak due to the consumption of Al. For the Y/Cr-modified aluminide coating, the corrosion products were mainly Al<sub>2</sub>O<sub>3</sub> after 200 h. Some weak peaks of TiO<sub>2</sub> and Ni<sub>3</sub>Al were identified.

Figure 10 shows the cross-sectional morphologies of the specimens after hot corrosion. A thick external scale formed on the cast alloy, as shown in Fig. 10a. Many inner sulfides were observed. In the mean time, a large amount of voids appeared, which led to a loose oxide scale.

For the aluminide coating, layered oxide scales were observed after 40 h (Fig. 10b) and the coating/substrate interface was illegible. EDS combined with XRD results indicated that the outmost was Ti-rich oxides layer, followed by an Al-rich oxides layer. Some inner oxides and sulfides appeared. According to EDS, the average Al content in the coating was less than 10 wt%, indicating that the coating could not be protective during the following test.

An alumina scale formed on the surface of the Y/Cr-modified aluminide coating after exposure for 200 h, as shown in Fig. 10c. The coating/substrate interface was still clear. The corrosion attack was only limited at the out part of the coating. As indicated by EDS, a small amount of inner oxides were observed, but no sulfides.

The surface morphologies of the Y/Cr-modified aluminide coating at different stages of the test are shown in Fig. 11. After 20 h, Al- and Cr- rich oxides formed simultaneously on the coating surface. The edges of these oxides were clear. After 200 h, however, intangibly morphology caused by the alkaline dissolution was



**Fig. 9** XRD patterns of the cast alloy and the coatings after hot corrosion

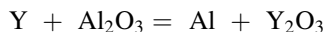
observed. According to EDS and XRD results, the corrosion products were mainly Al-rich oxides. No spallation was observed.

Figure 12 shows the elemental concentrations of the Y/Cr-modified aluminide coating after hot corrosion for 200 h. The result indicated that the surface of the coating was covered by an alumina scale. In the coating, two Cr-rich layers formed. The inner one located at the coating/substrate interface, mixed with the second-phases. Another Cr-rich layer formed at the out half of coating, underlying the oxide scale. A small amount of sulfides were observed in the oxide scale, still no S-rich phase appeared in the coating.

## Discussions

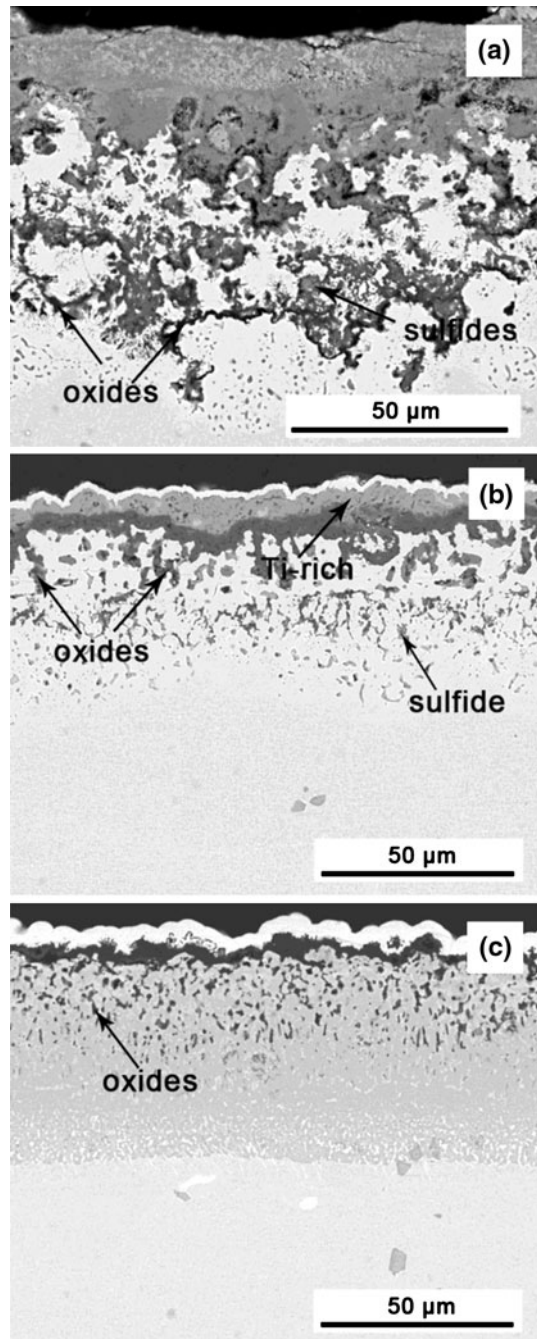
### Y/Cr-Modified Aluminide Coating

Based on the Y–Al phase diagram, the Y-rich phases formed after chromization were possibly AlY or  $\text{Al}_2\text{Y}_3$ . A similar result was reported by Tu et al. [11]. However, considering the formation mechanism of the chromized layer, we suggested that the Y-rich phases formed due to the reaction with the alumina powder during chromization. According to Godlewska et al. [14], chromization was mainly controlled by the outward diffusion of Ni to form a NiCr layer, Al in the substrate was not likely to diffuse outward. But, the metallic yttrium reacted with alumina as following reaction:



The formation free energy ( $\Delta G$ ) was  $-561.3$  kJ/mol at  $1050$  °C. So the reaction carried out spontaneously. This could be the Al supply to form these Y-rich phases. From this point of view, the Y-containing phases were trace because of the limited Y content in the slurry. This was, however, accordant with the scarce distribution of the yttrium on the  $\text{Ni}_2\text{Cr}_3$  layer.

**Fig. 10** Cross-sectional morphologies of the alloy and coatings after hot corrosion, **a** cast alloy for 20 h, **b** aluminide coating for 40 h, **c** Y/Cr-modified aluminide coating for 200 h



The aluminization was mainly controlled by the outward diffusion of Ni to form a NiAl layer, which was directly confirmed by the formation of an interdiffusion zone between the coating and substrate. However, this process, which was affected

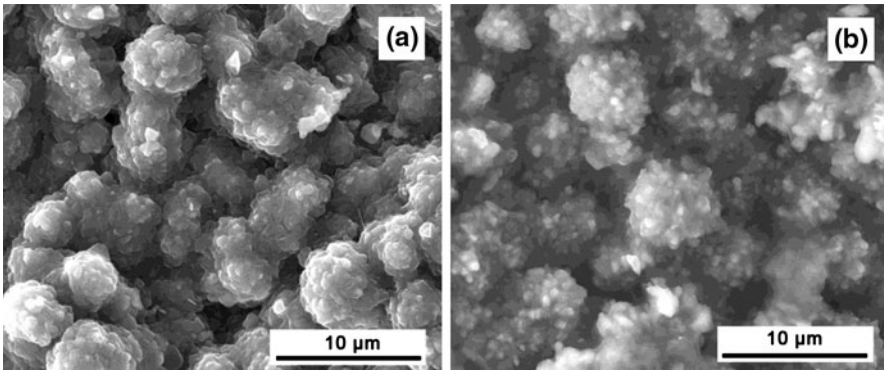


**Fig. 11** Surface morphologies of the Y/Cr-modified aluminide coating after hot corrosion, **a** after 20 h, **b** after 200 h

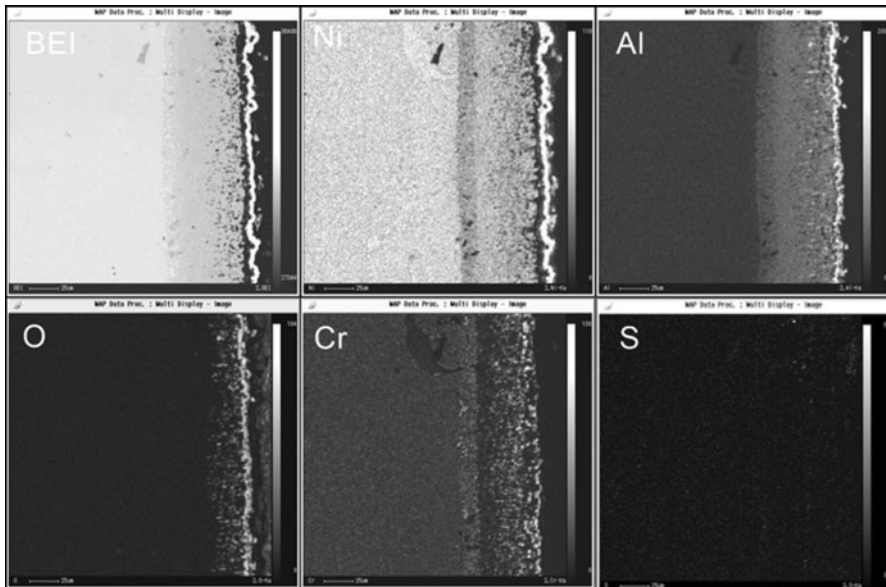


**Fig. 12** EPMA results of the Y/Cr-modified aluminide coating after hot corrosion

by the chromized layer, was not exactly the same as the typical HTLA (high temperature low activity) process [15]. A small amount of Cr-rich phases ( $\alpha$ -Cr,  $\text{AlCr}_{(x)}$ ) formed after aluminization. Based on the Ni–Al–Cr phase diagram at 1000 °C, Cr has a limited solubility in the  $\beta$ -NiAl phase, the excessive Cr led to the formation of  $\text{AlCr}_{(x)}$  phases during aluminization. But, too many  $\alpha$ -Cr or  $\text{AlCr}_{(x)}$  phases should be avoided in order to improve the ductility of the coatings/substrate system [16]. The yttrium had a very small solubility in a NiAl (less than 0.05 at%) or NiCrAl (less than 0.08 at%) alloy [17, 18]. Though the SIMS result confirmed the existence of yttrium in the coating, the exact quantity was still unknown.

Considering the detection limit of EPMA (less than 0.05 at%), the yttrium content should be in the desired range to form an adherent oxide scale.

### Cyclic Oxidation

In order to improve the oxidation resistance, alloys or coatings are expected to form an adherent oxide scale, which provides a barrier between the hot gas and the underlying metal. In the present study, the cast alloy suffered significant damage during the thermal cycling. According to Niu et al. [19], layered scales formed on the NiCrAl alloys during the high temperature exposure. These scales consisted of an outmost NiO layer, followed by a NiO layer containing some NiCr<sub>2</sub>O<sub>4</sub> and Ti-rich oxides, and an inner Cr-rich oxide layer. The cast alloy used in the present study followed this rule. The only difference was that the outmost NiO layer spalled during the thermal cycling.

For the coated specimens, Al<sub>2</sub>O<sub>3</sub> scales formed on both the coatings. But, the result indicated that the aluminide coating was less protective than the Y/Cr-modified aluminide coating. Two reasons were responsible for this. First, more Al were needed to heal the cracks and sustain the scale growth. Second, interdiffusion between the coating and substrate became significant with the time increasing. Both the reasons mentioned above led to a quick degradation of the  $\beta$ -NiAl phases in the aluminide coating. Correlatively, the volume of the coating changed big (about 13%) with the transformation from  $\beta$ -NiAl to  $\gamma'$ -Ni<sub>3</sub>Al [20]. Such a change contributed to the cracks and spallation of the oxide scales besides the thermal cycling factors [21].

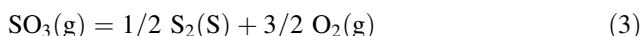
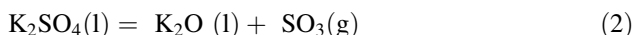
For the Y/Cr-modified aluminide coating, a higher mass gain was observed in the initial stage of exposure compared with the aluminide coating (Fig. 5). A possible reason was that the Y/Cr-modified aluminide coating had a relatively coarser surface, while the oxidation rate was calculated using a realistic geometry one. In the mean time, the Y and Cr additions, together with Al, joined the oxidation simultaneously at the beginning of the exposure, which also increased the mass gain.

The cyclic oxidation resistance of the Y/Cr-modified aluminide coating was improved. About the beneficial effects brought by the yttrium were discussed by many researchers [22–24]. The result in the present research was consistent with these studies. We suggested that, however, big atoms like Y and Cr (compared with Al) or their oxide particles concentrated in the grain boundaries changed the oxide growth mechanism by blocking the outward diffusion of metals to the surface. Thus, the inward diffusion of oxygen became the controlling process to form oxide scales. By this way, the oxide growth rate decreased. EPMA result indicated that a Cr-rich layer formed at the coating/substrate interface, which was different with the interdiffusion layer as formed in the aluminide coating for its high Cr content. This Cr-rich layer acted as a diffusion barrier between the coating and substrate, and slowed down the degradation of  $\beta$ -NiAl phases [25]. Consequently, the cyclic oxidation resistance of the Y/Cr-modified aluminide coating was better than that of the aluminide coating at 1000 °C.

## Hot Corrosion

The hot corrosion involves attacks by molten salts, such as  $\text{Na}_2\text{SO}_4$ ,  $\text{V}_2\text{O}_5$  and  $\text{NaCl}$ , which enter the turbine hot section as contamination from the air and fuel [26]. The molten salt mixture deposited on the coating surface would damage the oxide scale such as  $\text{Al}_2\text{O}_3$ ,  $\text{Cr}_2\text{O}_3$  and  $\text{SiO}_2$ . The general performances of these damages are those: oxide scales spallation, which are accelerated by the sulfidation or chlorination, and the dissolution of oxide scales in the alkaline or acidic environment.

In the present study, the salt mixture melted at 900 °C as following reactions:



The cast alloy didn't form a protective  $\text{Al}_2\text{O}_3$  or  $\text{Cr}_2\text{O}_3$  scale due to its low Al and Cr content. Consequently, sulfur and oxygen diffused through the oxide scale, and then inner sulfides and oxides formed. However, the sulfides were self-catalytic [27], re-sulfidation occurred in the substrate by the following reactions:



By this way, the internal sulfidation could continue without a further sulfur supply.

Both the coated specimens prolonged the service lifetime compared with the cast alloy. For the aluminide coating,  $\text{Al}_2\text{O}_3$  scale formed in the initial stage. But, accompany with the  $\text{Al}_2\text{O}_3$  dissolution in the alkaline environment generated by reaction (1) and (2), more Al were needed to grow the new oxide scale. This led to a quick consumption of the NiAl phases. In the mean time, according to reaction (3), the sulfur activity increased with the decrease of O to form  $\text{Al}_2\text{O}_3$  scale. The high sulfur partial pressure made S diffuse to the coating or substrate directly, and then inner sulfides formed. Similar rules with those for the cast alloy, re-sulfidation led to a quick disintegration of the aluminide coating, the coating was damaged completely after 60 h.

The Y/Cr-modified aluminide coating showed the best hot corrosion resistance due to the Y and Cr additions. It was recognized that the hot corrosion resistance was improved with the increase of the Cr content in the coating [28]. According to Lou [29], Cr-rich oxides mixed in the  $\text{Al}_2\text{O}_3$  scale were beneficial to prolong the service life for the coatings used in a salt-containing environment. Because,  $\text{Cr}_2\text{O}_3$  dissolved more easily than  $\text{Al}_2\text{O}_3$  in an alkaline environment, the dissolution rate of  $\text{Al}_2\text{O}_3$  decreased. It helped to form an  $\text{Al}_2\text{O}_3$  scale with a low Al consumption. The morphologies of the coating at different stage of the test (Fig. 11) indicated that the scale dissolution was the main damage during hot corrosion, no cracks were observed. The yttrium in the coating improved the scale adhesion in a sulfur-containing environment, which was consistent with the research by Amamo et al. [30]. Actually, the yttrium could form the high-melting phases, such as  $\text{YO}_x\text{S}_x$ ,

which proved to be chemical-stabilized. These phases fixed the sulfur in the oxide scale, and prevented its inward diffusion.

## Conclusions

The Y/Cr-modified aluminide coating which was free of the line-of-sight effect was prepared through a hybrid/pack cementation process. Cr and Y dissolved in the dominant  $\beta$ -NiAl phases. During the cyclic oxidation tests at 1000 °C, obvious cracks and spallation were observed on the surface of both the cast alloy and the aluminide coatings. But, a dense and adherent  $\text{Al}_2\text{O}_3$  scale with a low growth rate formed on the surface of the Y/Cr-modified aluminide coating. No degradation was observed in the coating. Hot corrosion behavior of the specimens coated with a 25 wt%  $\text{K}_2\text{SO}_4$  +75 wt%  $\text{Na}_2\text{SO}_4$  salt mixture were studied. O and S diffused through the oxide scales and formed inner oxides and sulfides for both the cast alloy (in 20 h) and the aluminide coatings (in 40 h). The Y/Cr-modified aluminide coating, however, was still protective after 200 h, no sulfides were observed in the coating. The scale dissolution was the main damage during the test. Cr and Y additions in the coating prevented the sulfur attack and the oxide scale spallation. In short, the Y/Cr-modified aluminide coating prepared in this study not only possessed good oxidation resistance, but also showed excellent hot corrosion performance.

**Acknowledgments** This project is financially supported by the Knowledge Innovation Program of the Chinese Academy of Sciences, Grant No. YYYJ-0912.

## References

1. C. Coddet, *Materials Science Form* **461**, 193 (2004).
2. W. Brandl, H. J. Grabke and D. Toma, *Surface and Coatings Technology* **86–87**, 41 (1996).
3. Y. N. Wu, G. Zhang, Z. C. Feng, and B. C. Zhang, *Surface and Coatings Technology* **138**, 56 (2001).
4. Y. J. Zhang, X. F. Sun, and Y. C. Zhang, *Materials Science and Engineering A* **360**, 65 (2003).
5. X. Ren and F. H. Wang, *Surface and Coatings Technology* **201**, 30 (2006).
6. B. Wang, J. Gong, A. Y. Wang, and C. Sun, *Surface and Coatings Technology* **149**, 70 (2002).
7. W. D. Costa, B. Gleeson, and D. J. Young, *Journal of Chemical Society* **141**, 2690 (1994).
8. W. D. Costa, B. Gleeson, and D. J. Young, *Surface and Coatings Technology* **88**, 165 (1996).
9. Z. D. Xiang, J. S. Burnell Grray, and P. K. Datta, *Surface Engineering* **17**, 287 (2001).
10. J. Jedlinski, K. Godlewski, and S. Mrowec, *Material Science and Engineering A* **121**, 5392 (1989).
11. D. C. Tu, C. C. Lin, S. J. Liao, and J. C. Chou, *Journal of Vacuum Science and Technology* **4**, 2601 (1986).
12. G. W. Goward and D. H. Boone, *Oxidation of Metals* **3**, 475 (1971).
13. F. H. Wang, H. Y. Lou, and L. X. Han, *Journal of Vacuum Science and Technology* **7**, 122 (1991).
14. E. Godlewska and K. Godlewski, *Oxidation of Metals* **22**, 117 (1984).
15. D. K. Das, S. V. Joshi, and V. Singh, *Metallurgical and Materials Transactions A* **29**, 2173 (1998).
16. F. D. Geib and R. A. Rapp, *Oxidation of Metals* **40**, 213 (1993).
17. E. W. A. Young and J. H. W. Dewit, *Oxidation of Metals* **26**, 351 (1986).
18. A. Kumar, M. Nasrallah, and D. L. Douglass, *Oxidation of Metals* **8**, 227 (1974).
19. Y. Niu, X. J. Zhang, Y. Wu, and F. Gesmundo, *Corrosion Science* **48**, 4020 (2006).
20. V. K. Tolpygo and D. R. Clarke, *Acta Materialia* **52**, 5115 (2004).
21. P. Y. Hou and A. P. Mat, *High Temperature* **22**, 535 (2005).
22. R. Cuffe, H. Buscaill, E. Caudron, C. Issartel, and F. Riffard, *Corrosion Science* **45**, 1815 (2003).

23. Z. Y. Liu and W. Gao, *Oxidation of Metals* **55**, 481 (2001).
24. W. Wang, P. Yu, and F. H. Wang, *Surface and Coatings Technology* **201**, 7425 (2007).
25. C. Bai, Y. Luo, and C. Koo, *Surface and Coatings Technology* **183**, 74 (2004).
26. J. Stringer, B. A. Wilcox, and R. I. Jaffee, *Oxidation of Metals* **5**, 11 (1972).
27. M. H. Li, X. F. Sun, and W. Y. Hu, *Oxidation of Metals* **65**, 137 (2006).
28. J. R. Nicholls, N. J. Simms, and W. Y. Chan, *Surface and Coatings Technology* **149**, 236 (2002).
29. H. Y. Lou, *Journal of Chinese society of corrosion and protection* **5**, 291 (1985).
30. T. Amamo, H. Isobe, N. Sakai, and T. Shishido, *Journal of Alloys and Compounds* **344**, 394 (2002).